Hydroxylammonium Nitrate: Synthesis, Cocrystals, and Properties

Supplementary Information

Andrew J. Bennett,[a] Haley R. Froberg,[a] Michael K. Bellas,[b] Leila M. Foroughi,[a] and Adam J. Matzger*[a,c]

[a] Department of Chemistry, University of Michigan, 930 North University Avenue, Ann Arbor, Michigan 48109, United States

[b] Research Department, Chemistry Division, United States Navy – Naval Air Systems Command (NAVAIR). Naval Air Warfare Center, Weapons Division (NAWCWD), 1900 N. Knox Road, China Lake, California, 93555, United States

[c] Macromolecular Science and Engineering Program, University of Michigan, 930 North University Avenue, Ann Arbor, Michigan 48109, United States

Table of Contents

SI 1. Experimental

Caution: Although no unplanned detonations were encountered during this work, HAN is a powerful energetic oxidizer and many of the cocrystals produced are potent explosives with high impact sensitivity. Be aware that the potential for severe injury exists if these materials are handled improperly. Grinding experiments were conducted while wearing steel-woven Kevlar gloves and a protective face shield.

Hydroxylammonium chloride (HACl) and 3,5-diamino-1H-1,2,4-triazole were obtained from Acros Organics. Silver nitrate, isoquinoline N-oxide, and urea were obtained from Sigma Aldrich. 4,4'-Bipyridine-1,1'-dioxide and 2,4-dihydro-3H-1,2,4-triazol-3-one were obtained from AmBeed. 3-Amino-1H-1,2,4-triazole was obtained from Alfa Aesar. 1,10-Phenanthroline was obtained from TCI. 5-Amino-tetrazole monohydrate was purchased from Sigma Aldrich and dehydrated under vacuum. 3-Amino-5-nitro-1H-1,2,4-triazole was obtained from NAVAIR, Naval Air Warfare Center Weapons Division, China Lake. Pyrazine-1,4-dioxide was prepared using the published method.(1)

Synthesis of Hydroxylammonium Nitrate

The following steps must be completed while minimizing exposure to moisture. All reagents were pre-dried under vacuum and all material transfers were completed in a nitrogen glovebox. To a 100 mL round-bottom flask was added HACl (1027 mg, 14.77 mmol), silver nitrate (2519 mg, 14.77 mmol), and anhydrous ethanol (25 mL). The reaction was allowed to stir at room temperature under nitrogen for one hour, after which time the silver chloride precipitate was filtered off and the filtrate dried down under flowing nitrogen. The solid was then transferred to a sublimation apparatus and vacuum was applied (20.0 mTorr). Sublimation proceeded with the introduction of dry ice to the cold finger followed by a gradual heating of the sublimation chamber to 50 °C over the course of one hour. Complete sublimation of the solid occurred within that time. The sublimation chamber was left under vacuum overnight to ensure complete dryness of the sublimate. HAN (1376 mg, 14.33 mmol, 97% yield) was collected under a nitrogen atmosphere by gentle scraping of the cold finger with a plastic spatula and stored in a Schlenk flask under nitrogen.

Synthesis of HAN Cocrystals

Each HAN cocrystal was generated through both melt fusion and dry grinding. Slurry crystallization was utilized in some cases to generate higher quality crystals for single-crystal X-ray diffraction.

Melt Fusion

General procedures for melt fusion are as follows. To a 1.5 mL Eppendorf tube was added HAN (5-10 mg) and coformer (0.5/1/2 molar equivalents). The order of addition was not found to be important and no mixing was performed. The Eppendorf tube was heated to 50 °C for one hour in a 300 rpm orbital shaker and then slowly cooled to 20 °C over 12 hours with continuous agitation. Final products generally consisted of powder and clumped, irregular crystals.

Slurry Cocrystallization

Slurry cocrystallization was utilized to generate higher quality crystals for HAN:5-AT, HAN:PA, HAN:BPDO, HAN:ANTA, and HAN:Urea. General procedures were performed under nitrogen atmosphere as follows. To a 1.5 mL vial was added 150 µL of isopropanol saturated with HAN. The target coformer, finely ground, was added in consecutive additions of 1-2 mg until a small amount of excess solid remained

undissolved. Another 1-2 mg of solid HAN was added and the samples left on an orbital shaker. High quality single crystals formed within one day.

Characterization

Single-Crystal Structure Determination
Single-crystal X-ray diffraction data were collected using a Rigaku XtaLAB Synergy-S X-ray diffractometer with a kappa goniometer geometry configuration. The X-ray source is a PhotonJet-S microfocus Cu source (λ = 1.54184 Å) operated at 50 kV and 1 mA. X-ray intensities were measured with a HyPix-6000HE detector held 34 mm from the sample. The data were processed using CrysAlisPro v40.82 (Rigaku Oxford Diffraction) and were corrected for absorption. The structures were determined and refined using OLEX2(2) v1.5-ac5-024 with SHELXT(3) and SHELXL.(4) All non-hydrogen atoms were refined anisotropically with hydrogen atoms located in idealized positions.

Powder X-Ray Diffraction
All powder pattern data (except for HAN and HAN:Urea; see below) were collected using a Panalytical Empyrean system utilizing Cu-Kα radiation (λ = 1.54184 Å) and operating at 45 kV and 40 mA. The system uses a Bragg-Brentano HD X-ray optic and an X'Celerator Scientific detector operating in a continuous 1D scan mode. Scans were conducted according to the following parameters: 2θ = 5° to 50°, step size = 0.008°, and step speed = 20 seconds. The data were plotted using Origin Pro 2021b. Powder pattern data for HAN and HAN:Urea were collected using the Rigaku XtaLAB Synergy-S X-ray diffractometer described above. Samples were loaded into <1 cm lengths of polyimide tubing with 0.5mm inner diameter and the ends sealed with clay to protect against moisture. Powder patterns were collected in powder mode from 2θ = 5° to 40° with 2% beam intensity, 2000s exposure time, and a detector distance of 100mm. The data were plotted using Origin Pro 2021b.

Differential Scanning Calorimetry (DSC)
Differential scanning calorimetry (DSC) thermograms were recorded on a TA Instruments Q20 DSC instrument. General experiments were carried out at a heating rate of 5 °C/min, covering a temperature range of 5 °C to 400 °C. Melt cycle experiments were carried out at a heating rate of 5 °C/min from 20 °C to 100 or 120 °C with a ten-minute isothermal hold at the peak temperature before cooling back to 20 °C and repeating the cycle 9 times. Samples were prepared in Tzero™ hermetic aluminum DSC pans. The instrument was calibrated using an indium standard, all DSC thermograms were analyzed using TA Universal Analysis 2000, V4.5A, build 4.5.0.5 and plotted using Origin Pro 2021b.

Thermogravimetric Analysis (TGA)
Thermogravimetric analysis (TGA) thermograms for each sample were recorded on a TA Instruments Q50 TGA. General experiments were conducted in platinum TGA sample pans under a nitrogen purge of 50 mL/min with a heating rate of 10 °C/min, covering a temperature range of 22 °C to 800 °C. Isothermal experiments were conducted with a heating rate of 10 °C/min to the target temperature and held for up to 48 hours under a nitrogen purge of 50 mL/min. The instrument was calibrated using the Curie points of alumel and nickel standards and all TGA thermograms were analyzed using TA Universal Analysis 2000, V4.5A, build 4.5.0.5. The data were plotted using Origin 9.85.

Dynamic Vapor Sorption (DVS)
Dynamic vapor sorption (DVS) experiments were performed using a Q5000 SA Dynamic Vapor Sorption Analyzer. Sample mass was monitored from 5-90% relative humidity with a step size of 2%, where

relative humidity was stepped once sample mass stabilized (<0.01% change for 2 minutes) with a maximum of 120 minutes equilibration time per step and starting from initial masses of 3-10 mg. In the case of HAN, a pre-drying step was introduced in which the sample was held at 35 °C and 0% relative humidity for 24 hours prior to data collection. The data were analyzed using TA Universal Analysis 2000, V4.5A, build 4.5.0.5 and plotted using Origin Pro 2021b.

Raman Spectroscopy

Raman spectra were collected using a Renishaw inVia Raman Microscope equipped with a Leica microscope and a 633 nm laser. Spectra were collected in static scan mode with a range of 430-1592 cm^{-1} with 1800 lines/mm gratings, 50 µm slit size, and a Renishaw Centrus 2GRX02 detector. Calibration was performed using a silicon standard. The data were plotted using Origin Pro 2021b.

Impact Sensitivity

Impact sensitivities were determined using an in-house apparatus in which a 2.380 Kg stainless steel weight is dropped from varying heights onto a 2 mg +/- 10% sample housed in an aluminum DSC pan resting upon an anvil. In the case of HAN, the DSC pans were prepared and hermetically sealed under a nitrogen atmosphere. 20 samples of each material were tested and the Dh50 calculated as the drop height at which there was a 50% probability of detonation.

Microwave plasma atomic emission spectroscopy

Microwave plasma atomic emission spectroscopy data was collected using an Agilent 4210 MP-AES system and analyzed with MP Expert version 1.6.1. The instrument was calibrated using silver nitrate solutions at 0.05, 0.5, 1, and 2 ppm silver in 5% nitric acid with an R2 of 0.99999. HAN (100-200 mg) samples were dissolved in 2 mL of 5% nitric acid.

SI 2. Crystallographic Data

Table S1. Crystallographic parameters for HAN cocrystals

	HAN:ANTA	HAN:3-AT	HAN:5-AT	HAN:DAT	HAN:BPDO	2HAN:PDO	HAN:PA	HAN:TO	HAN:Urea
stoichiometry	1:1	1:1	1:1	1:1	1:1	2:1	1:1	1:1	1:1
space group	$P2_1/c$	$Pca2_1$	$Pna2_1$	$P2_1/c$	$P2_1/n$	$P2_1/n$	$P1$	$Pca2_1$	$P2_1$
a (Å)	15.1073(3)	11.7993(3)	17.5879(5)	10.5441(4)	7.2509(3)	5.98412(14)	10.4611(3)	18.1310(4)	3.71414(12)
b (Å)	8.0654(2)	3.60659(8)	3.67189(9)	8.1023(3)	16.9335(7)	16.1555(4)	10.8576(3)	3.67557(10)	9.2773(3)
c (Å)	7.00820(10)	17.0814(4)	10.8826(3)	19.1221(8)	10.1908(3)	6.29928(14)	11.9263(3)	10.7747(3)	9.4655(3)
α (°)	90	90	90	90	90	90	75.709(2)	90	90
β (°)	98.474(2)	90	90	103.452(4)	98.392(3)	94.922(2)	86.876(2)	90	95.516
γ (°)	90	90	90	90	90	90	72.457(3)	90	90
Volume (Å^3)	844.602	726.903	702.807	1588.81	1237.86	606.746	1251.36	718.045	324.644
ρ_{calc} (g cm^{-3})	1.758	1.646	1.712	1.632	1.525	1.665	1.466	1.675	1.597
formula	$C_2H_7N_7O_6$	$C_2H_8N_6O_4$	$CH_7N_7O_4$	$C_4H_{18}N_{14}O_8$	$C_{10}H_{12}N_4O_6$	$C_4H_{12}N_6O_{10}$	$C_{24}H_{24}N_8O_8$	$C_2H_7N_5O_5$	$CH_8N_4O_5$
fW (g/mol)	225.12	180.12	181.11	390.27	284.23	304.17	552.5	181.11	156.1
crystal system	monoclinic	orthorhombic	orthorhombic	monoclinic	monoclinic	monoclinic	triclinic	orthorhombic	monoclinic
Z	4	4	4	4	4	4	2	4	2
$R_{int.}$ (%)	2.27	2.43	2.81	2.43	3.91	1.84	2.66	2.24	2.27
R_1/R_{W2} (%)	3.05/8.37	3.12/8.54	3.55/8.36	3.83/12.31	5.72/15.19	3.81/11.27	4.18/14.36	2.63/7.47	2.97/8.12

SI 3. Thermal Ellipsoid Plots at 50% Probability

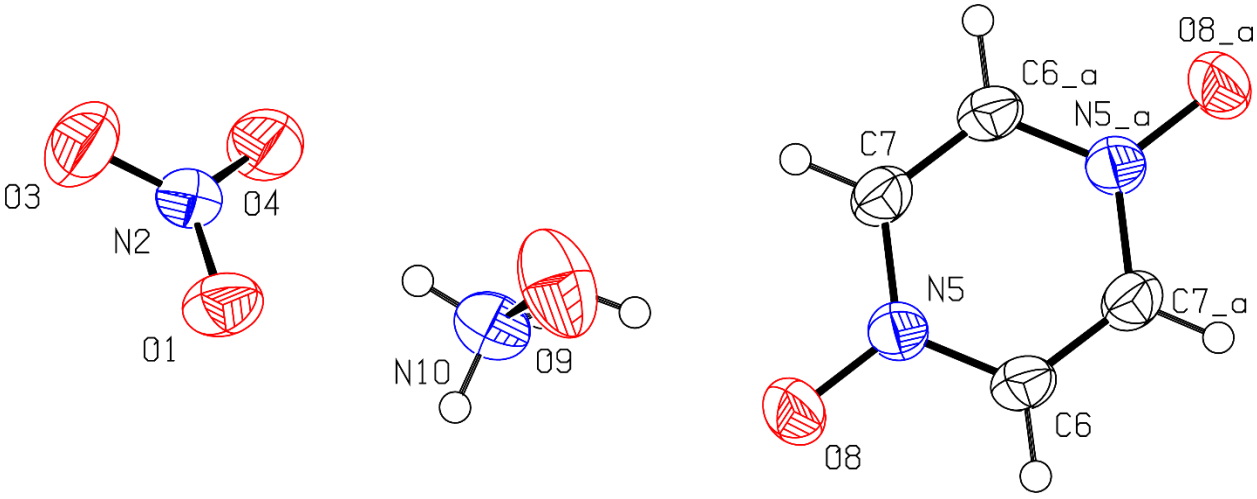

Figure S1. Thermal ellipsoid plot of 2HAN:PDO and 293(2) K.

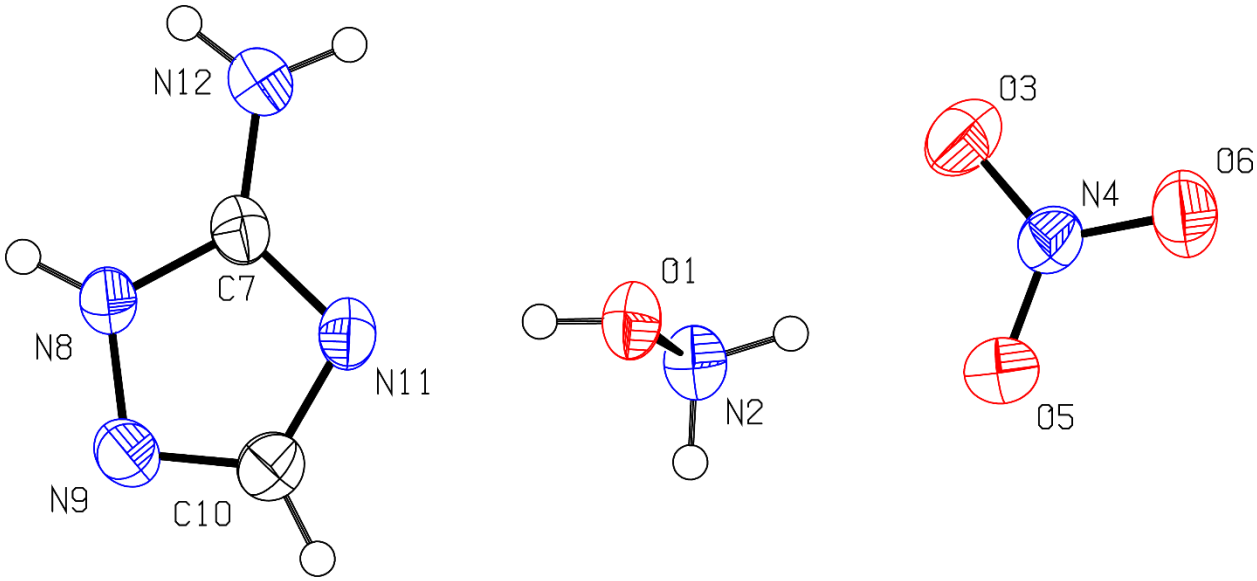

Figure S2. Thermal ellipsoid plot of HAN:3-AT and 293(2) K.

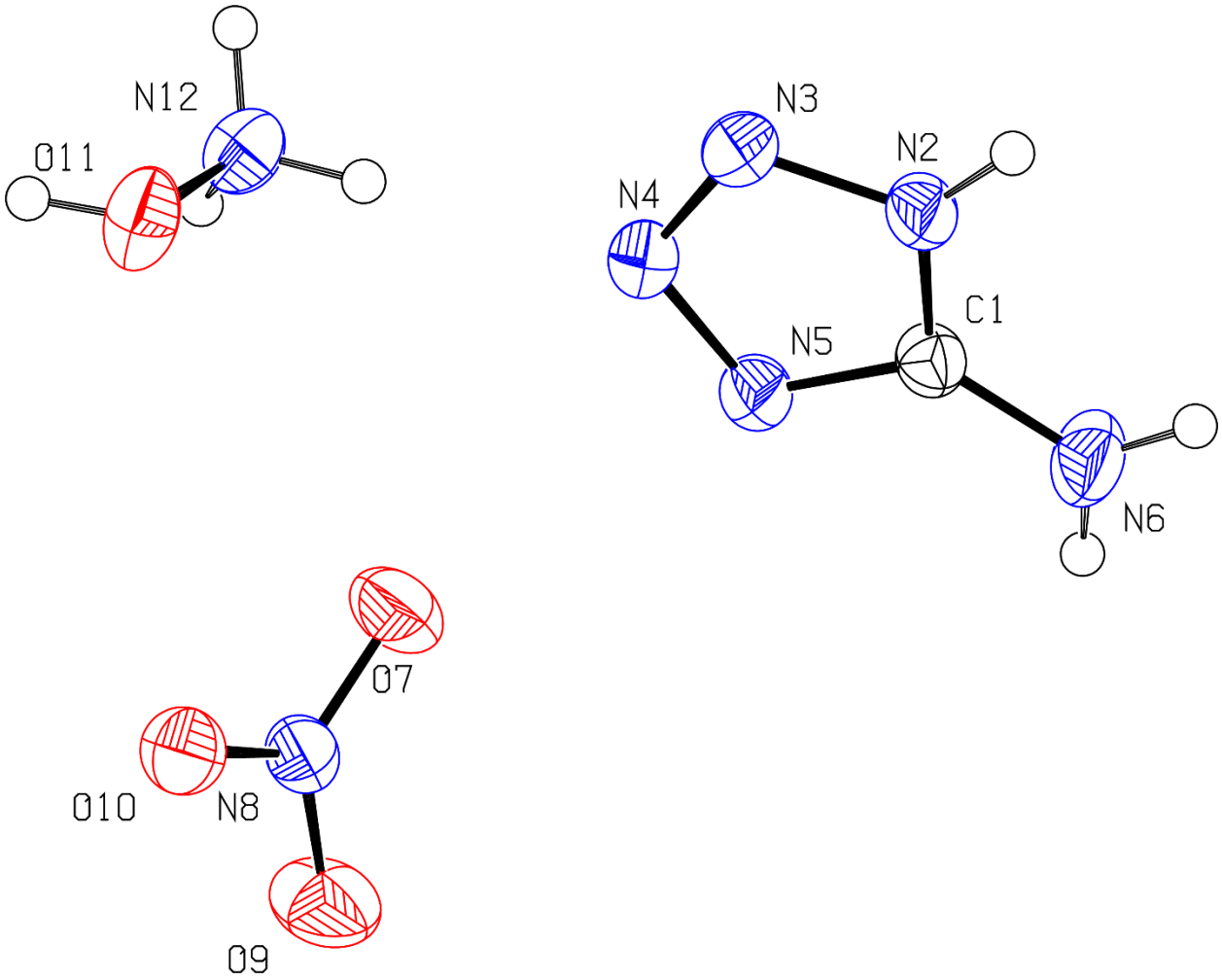

Figure S3. Thermal ellipsoid plot of HAN:5-AT and 293(2) K.

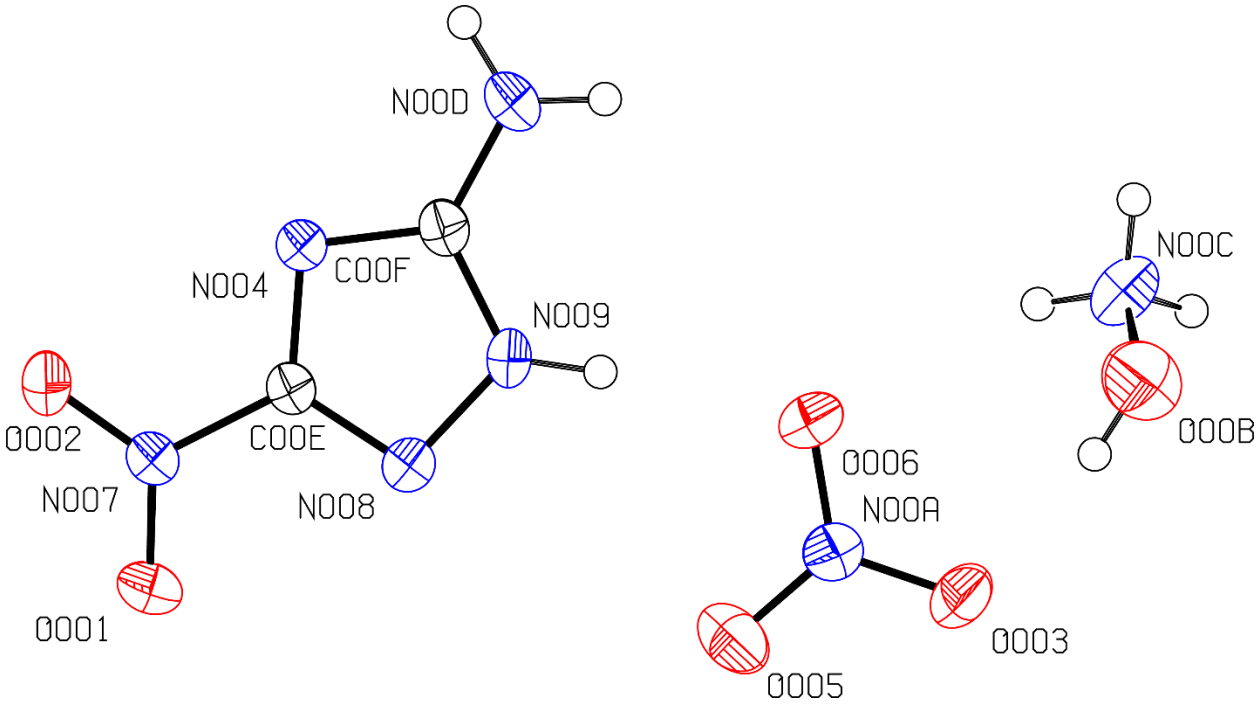

Figure S4. Thermal ellipsoid plot of HAN:ANTA at 293(2) K.

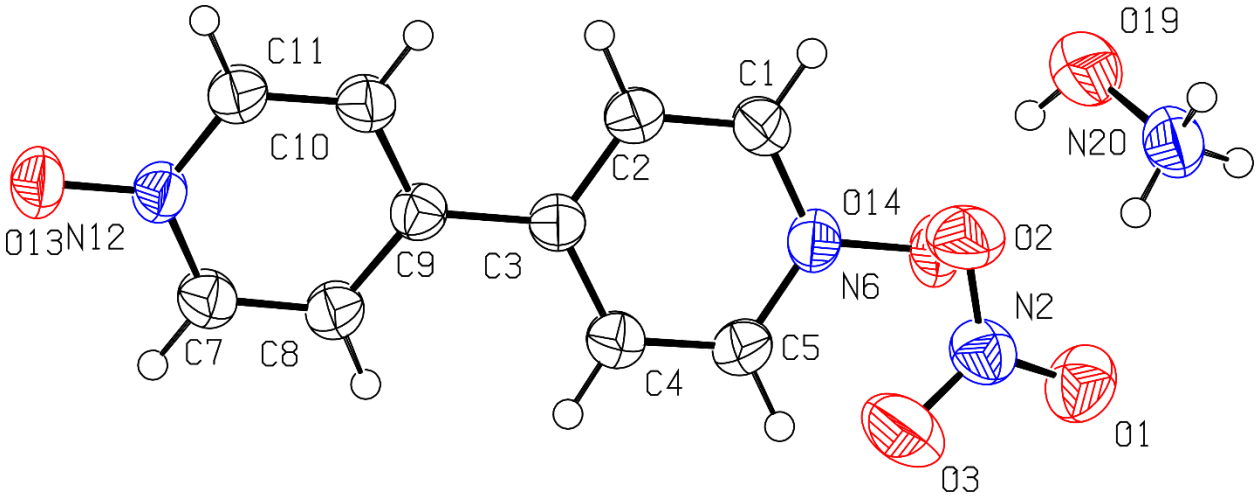

Figure S5. Thermal ellipsoid plot of HAN:BPDO at 293(2) K.

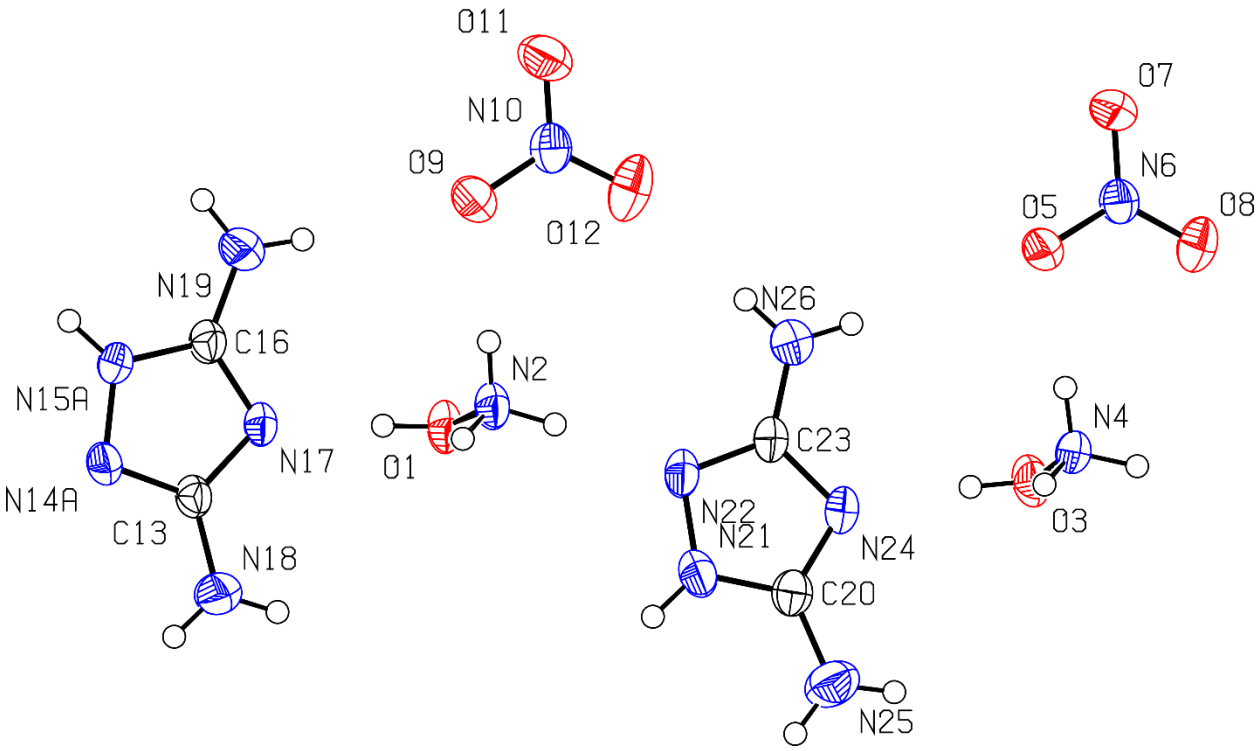

Figure S6. Thermal ellipsoid plot of HAN:DAT at 293(2) K.

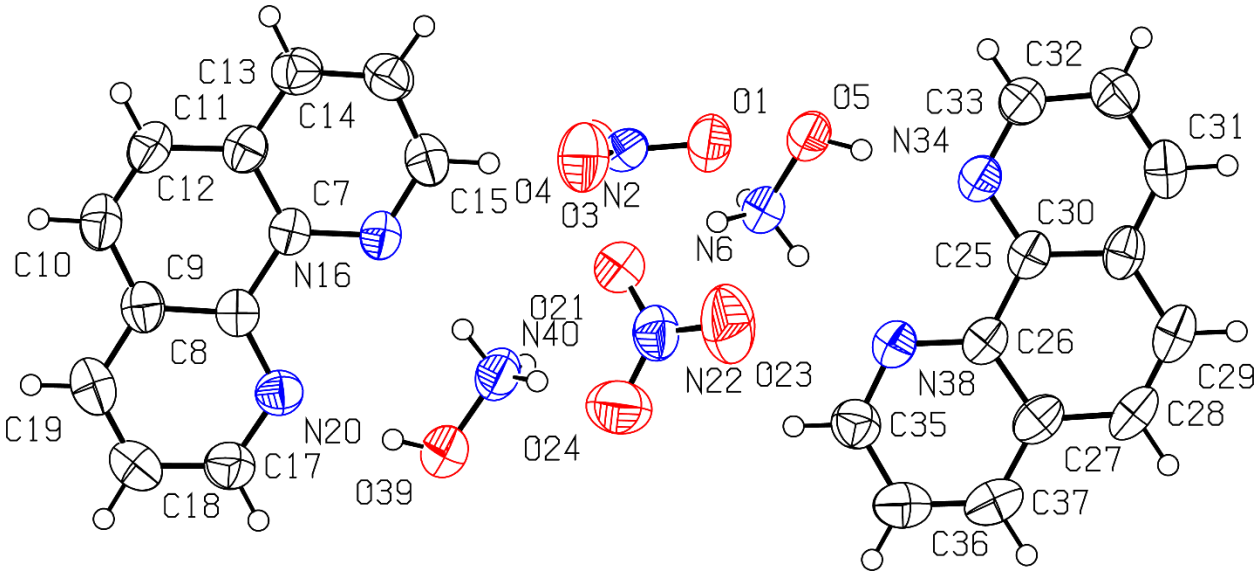

Figure S7. Thermal ellipsoid plot of HAN:PA at 293(2) K.

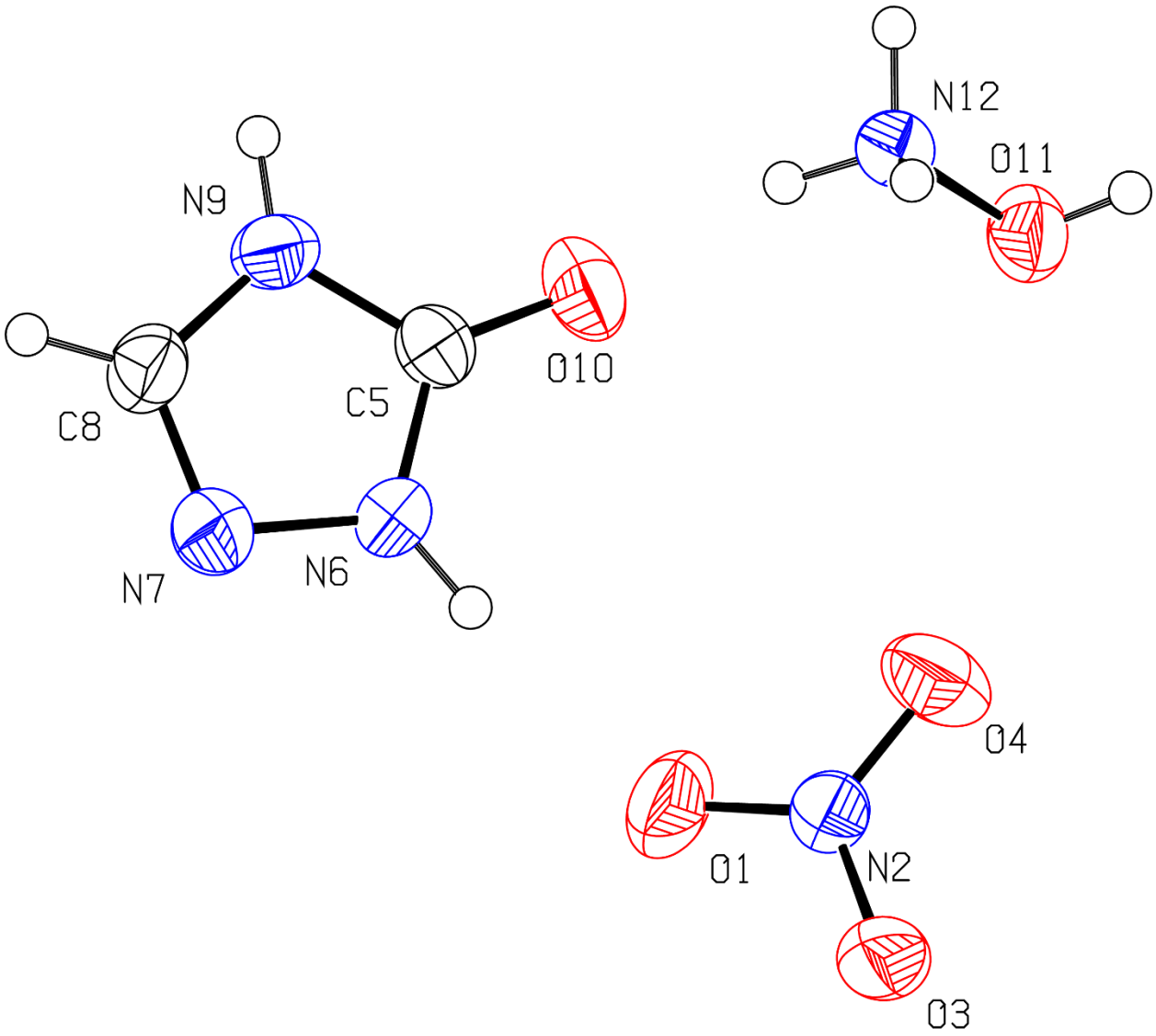

Figure S8. Thermal ellipsoid plot of HAN:TO at 293(2) K.

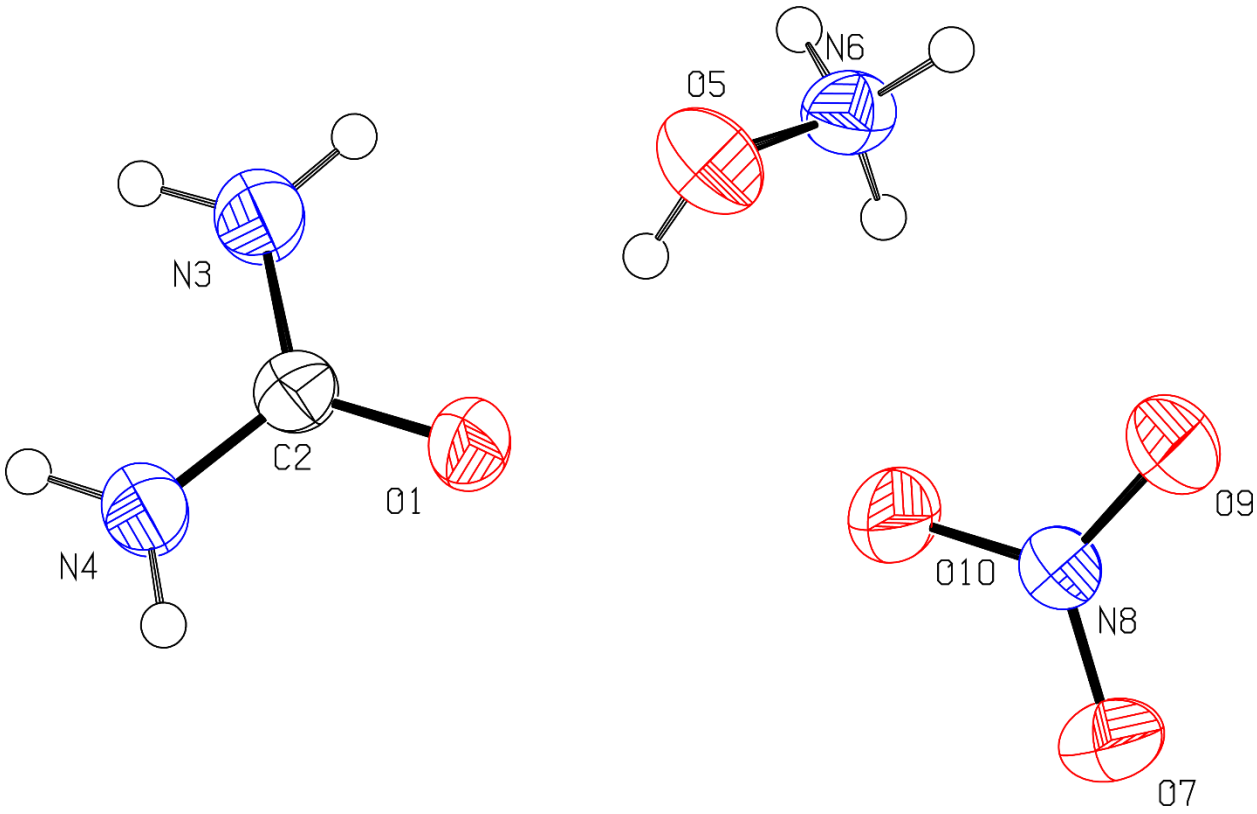

Figure S9. Thermal ellipsoid plot of HAN:Urea at 293(2) K.

S4. PXRD Data

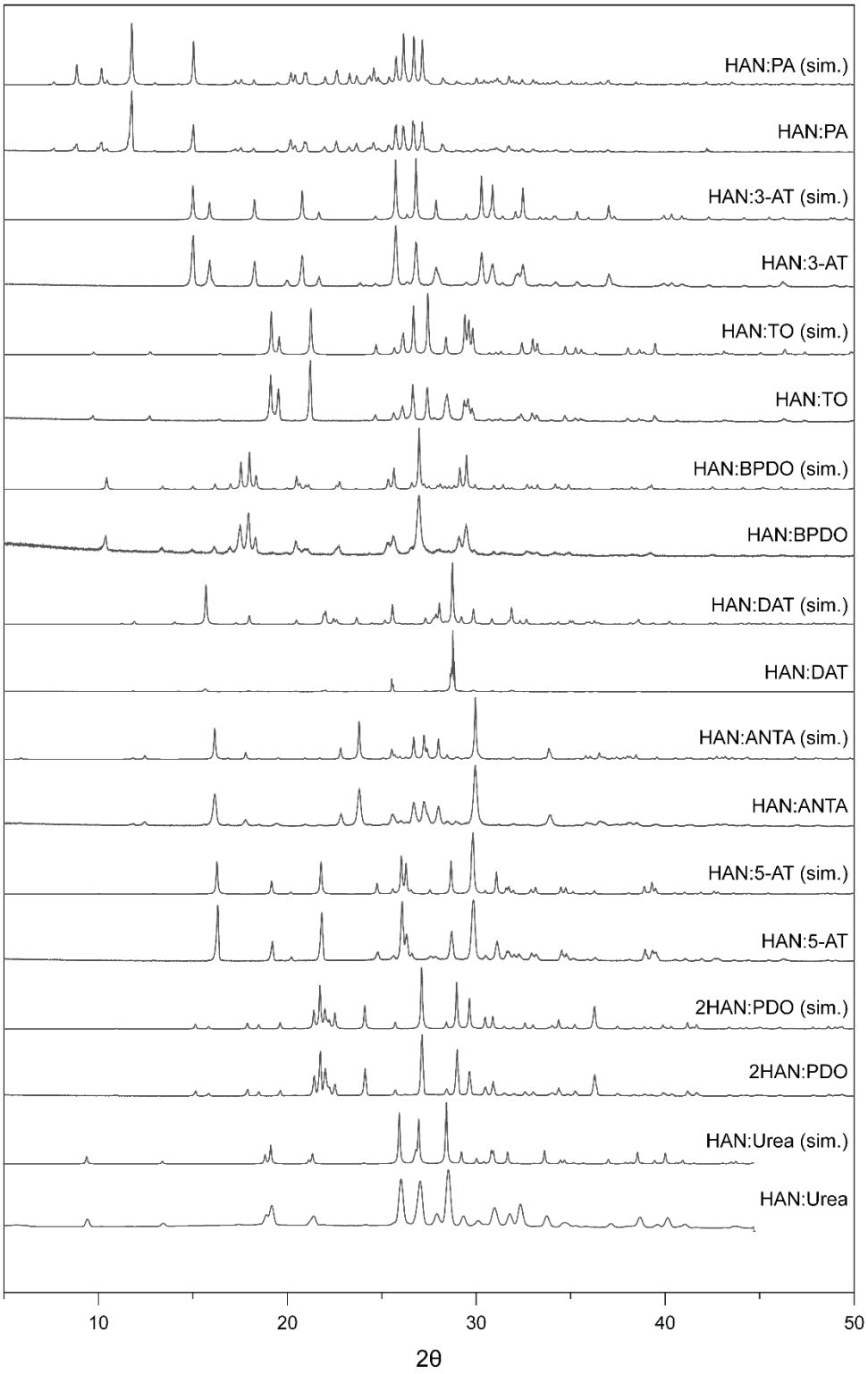

Figure S10. Experimental and simulated power patterns of HAN ionic cocrystals.

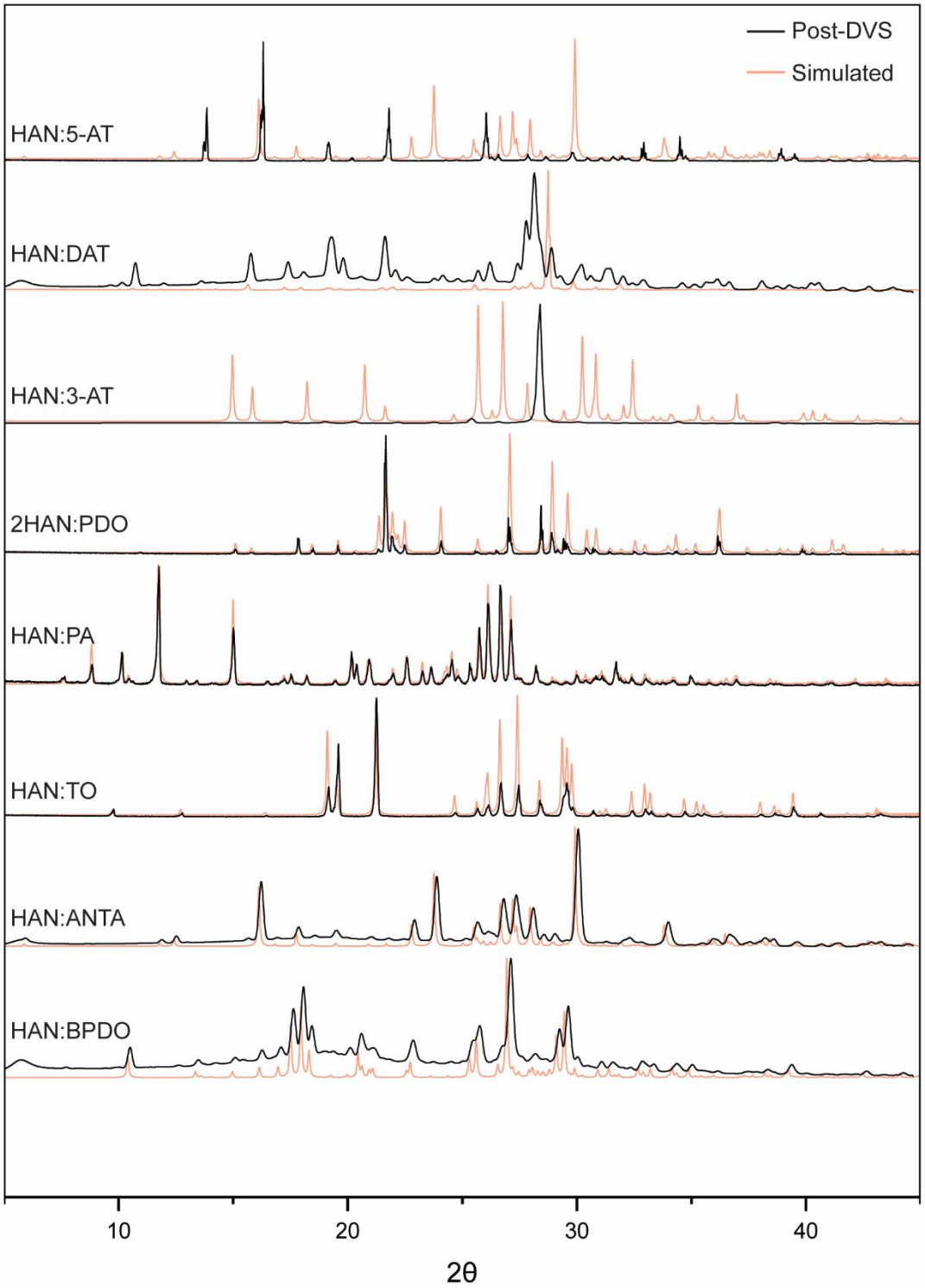

Figure S11. Powder patterns taken after DVS experiments overlaid with simulated powder patterns of the ionic cocrystals. HAN:DAT, HAN:5-AT, and HAN:3-AT differ from the simulated patterns.

S5. Raman Spectra

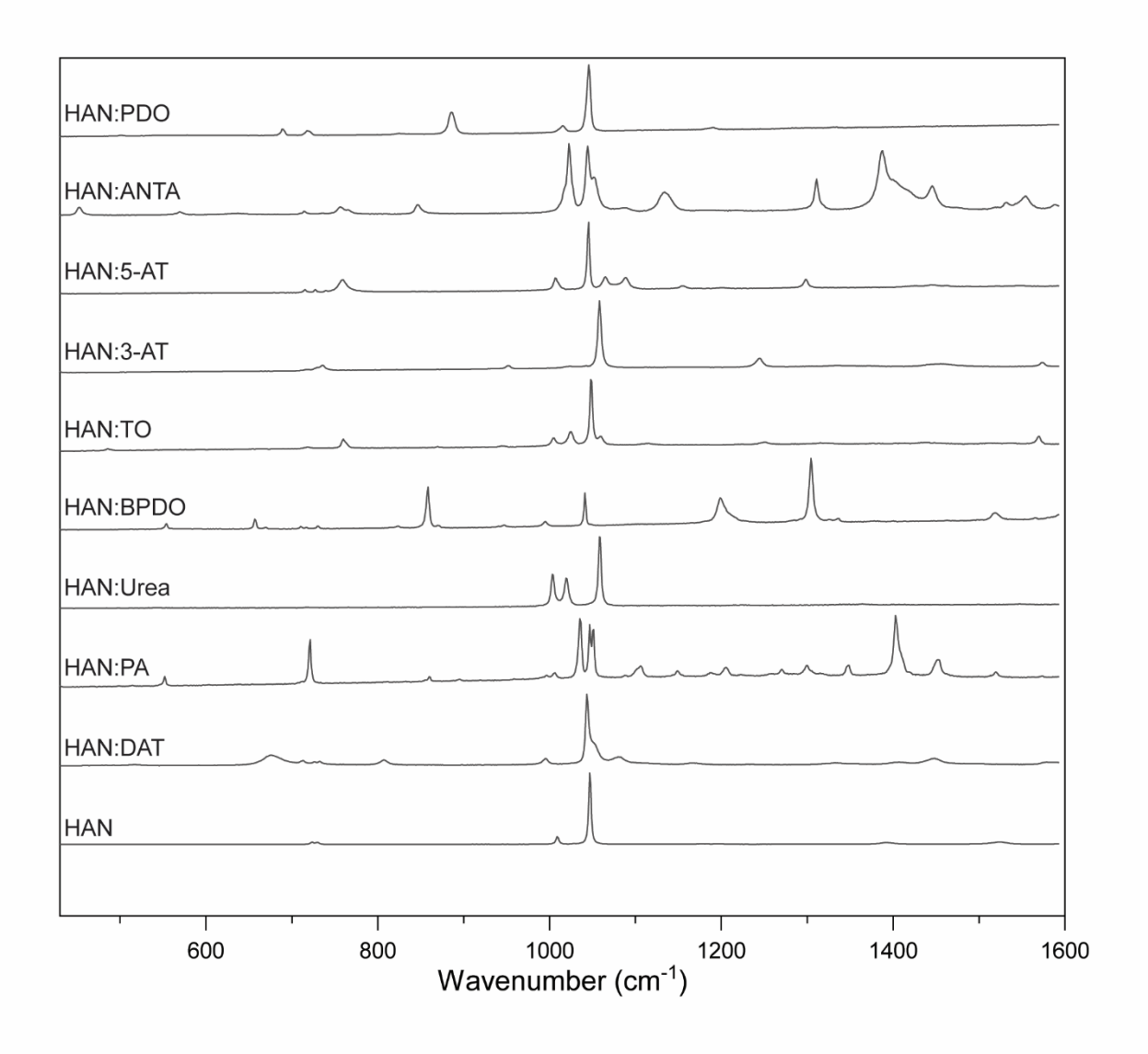

Figure S12. Raman spectra of HAN and HAN ionic cocrystals.

S6. Thermal Data

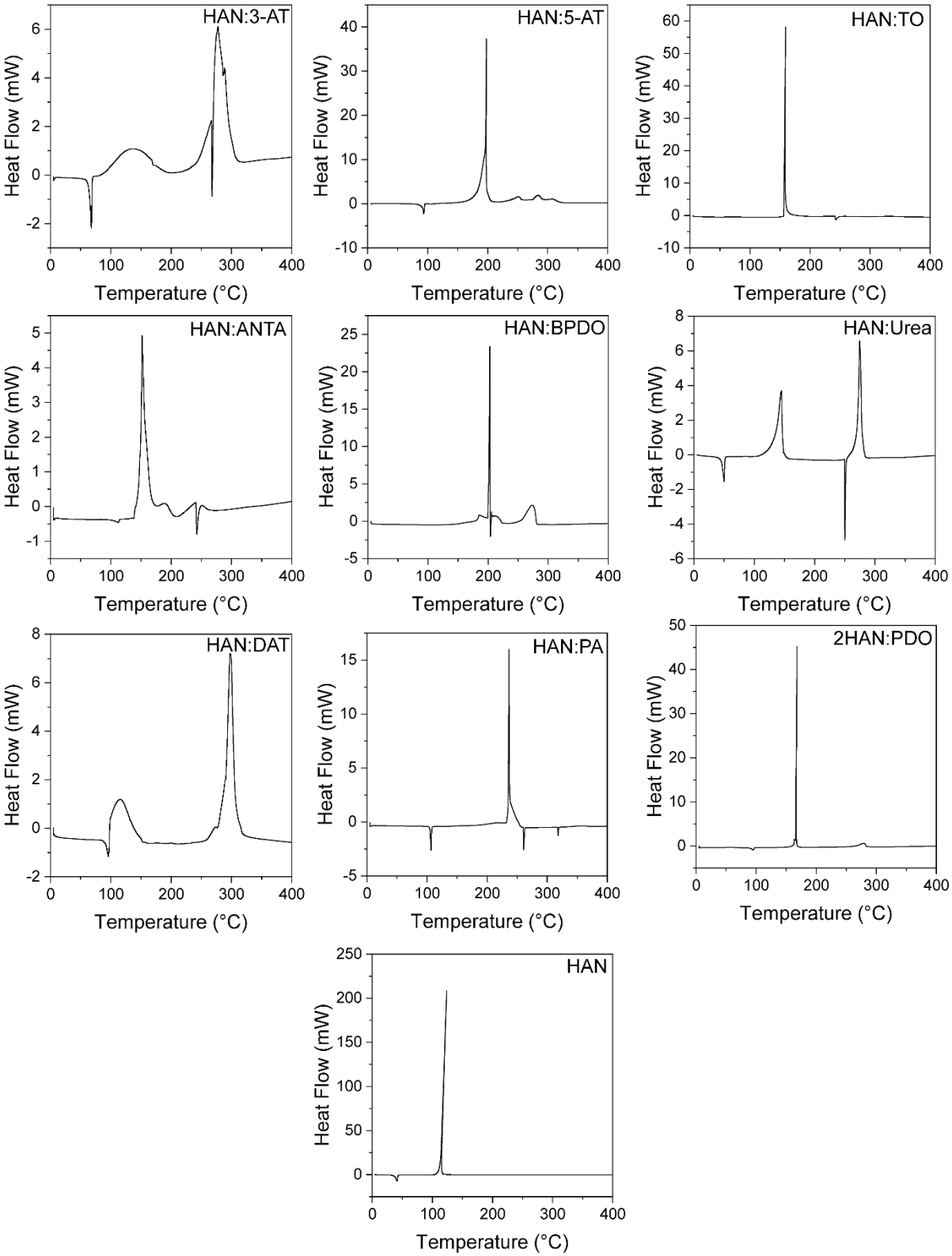

Figure S13. Differential scanning calorimetry traces for HAN and HAN ionic cocrystals.

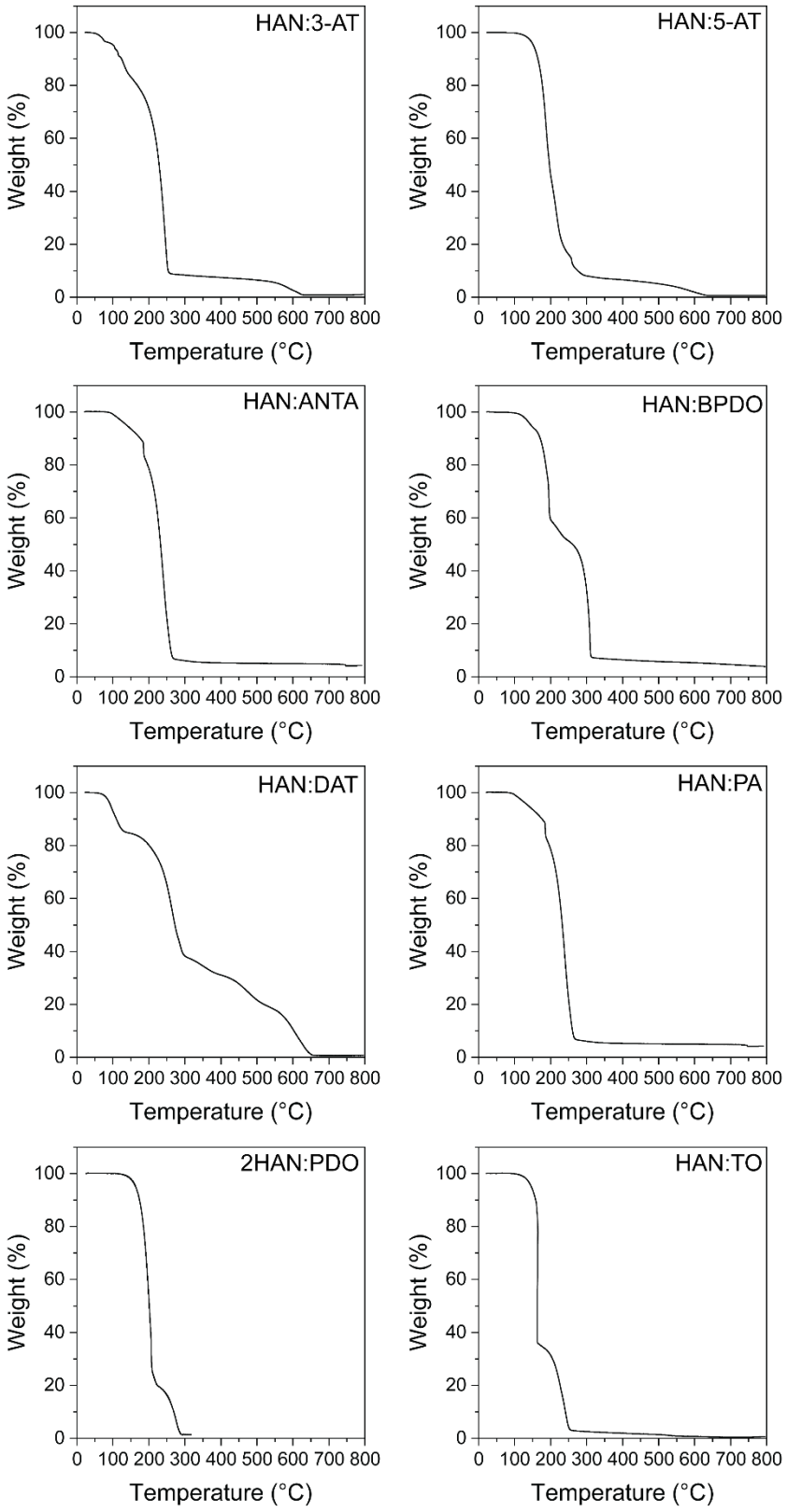

Figure S14. Thermogravimetric analysis traces for HAN ionic cocrystals.

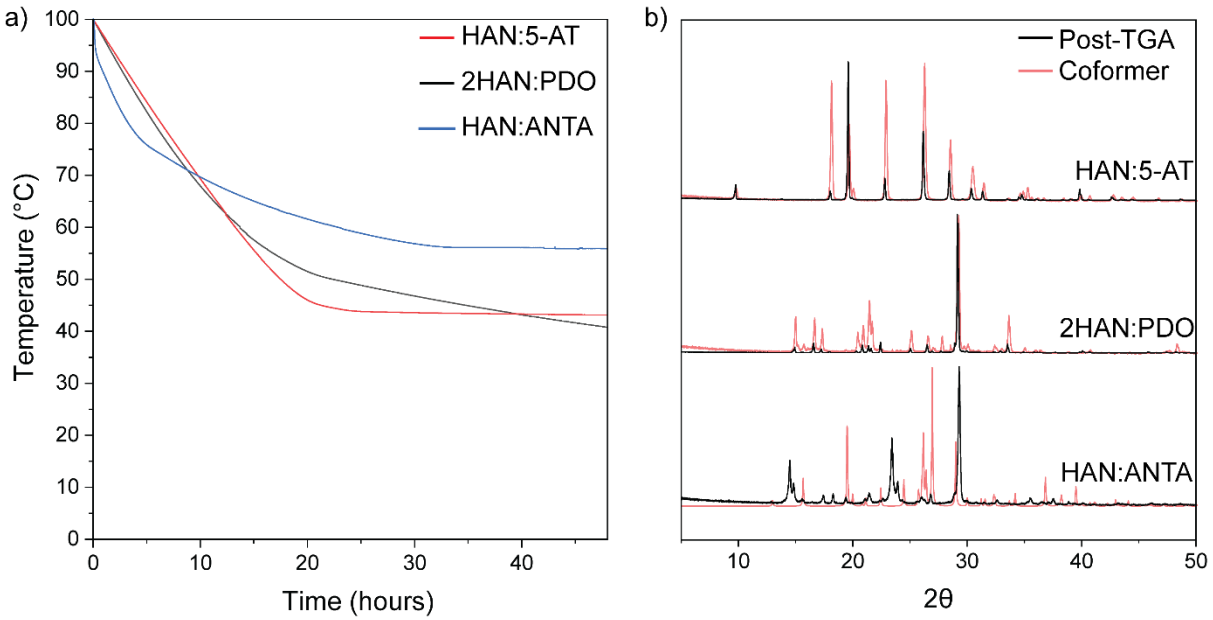

Figure S15. a) Overlaid isothermal TGA plots of three energetic HAN cocrystals held at 100 °C for 48 hours, and b) powder patterns of the same samples after the TGA experiment overlaid with the powder patterns of the coformer molecules.

SI 7. Predicted BFDH Morphology

BFDH morphology was calculated for each cocrystal using Mercury 2025.1.1 (Build 448738).

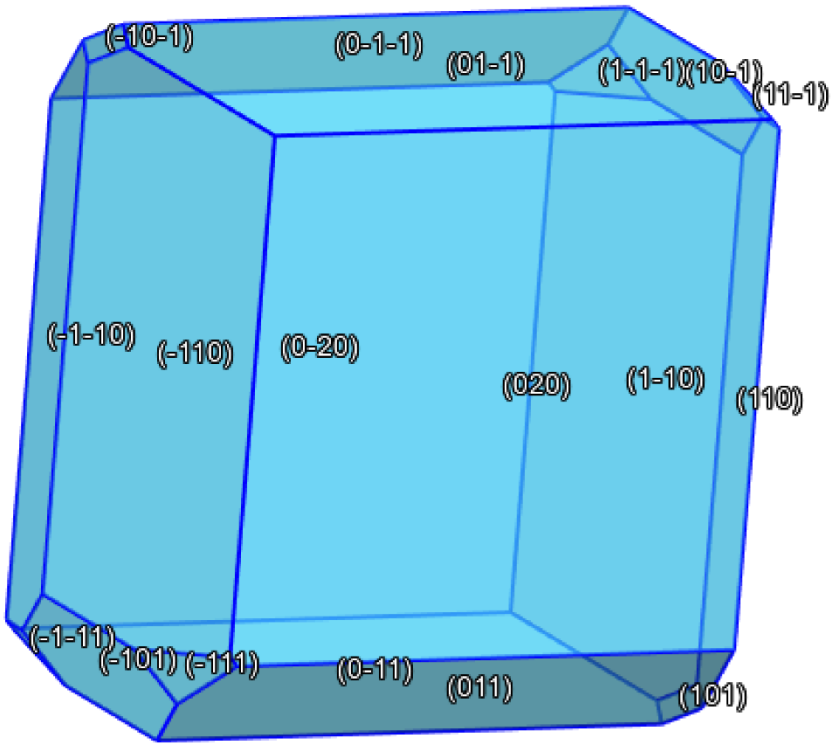

Figure S16. Predicted BFDH morphology for 2HAN:PDO.

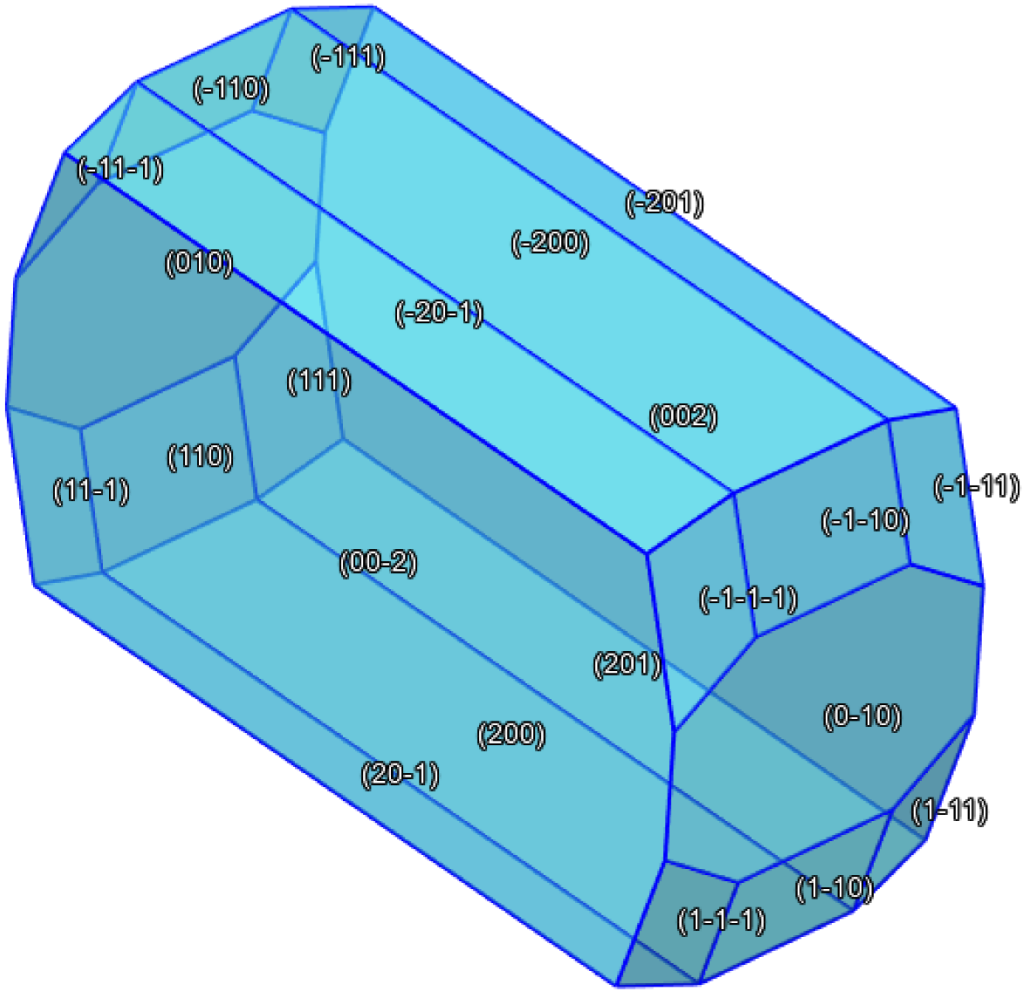

Figure S17. Predicted BFDH morphology for HAN:3-AT.

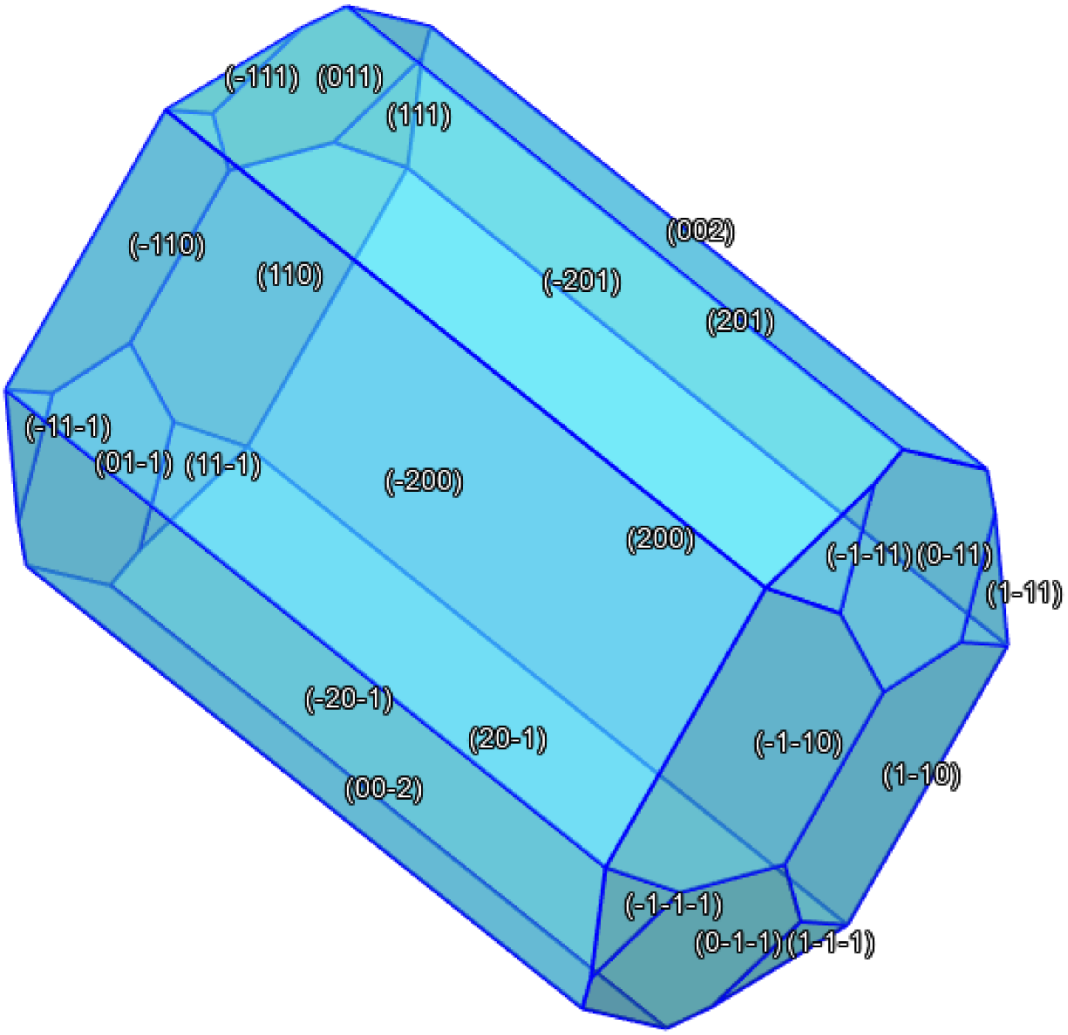

Figure S18. Predicted BFDH morphology for HAN:5-AT.

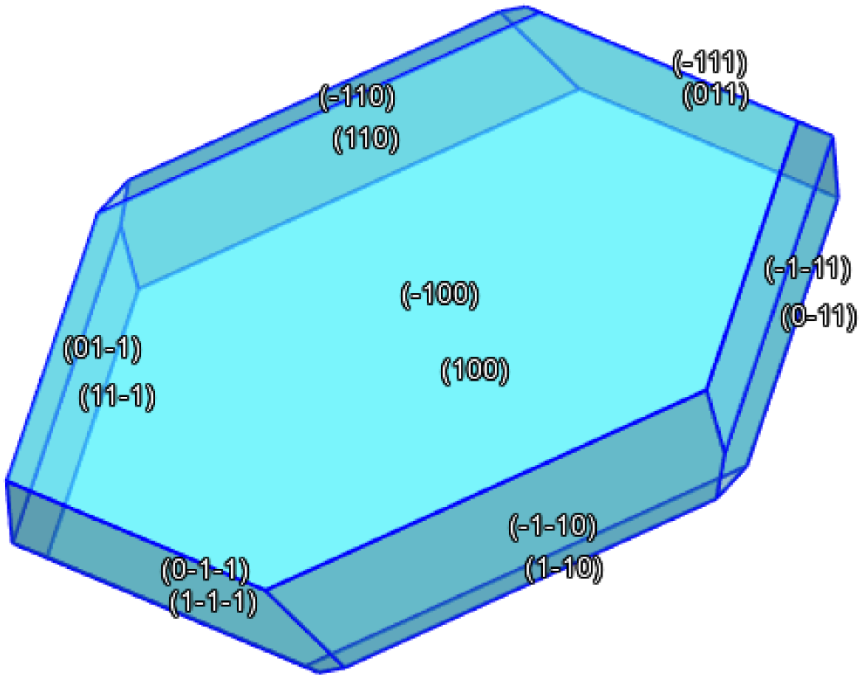

Figure S19. Predicted BFDH morphology for HAN:ANTA.

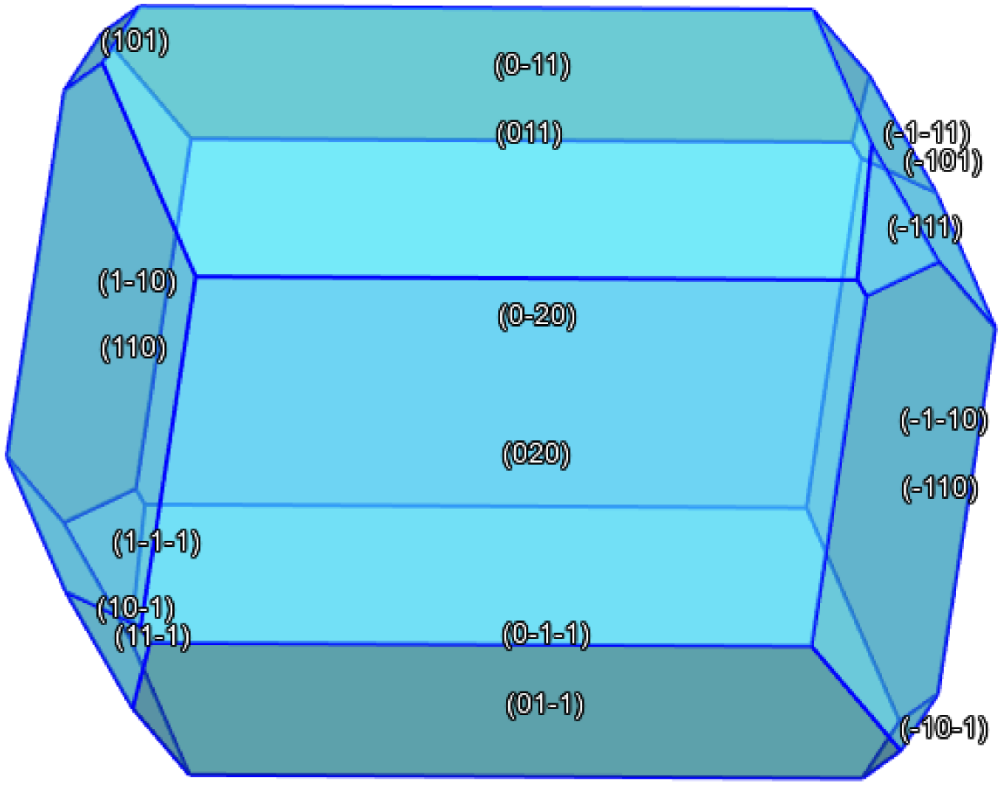

Figure S20. Predicted BFDH morphology for HAN:BPDO.

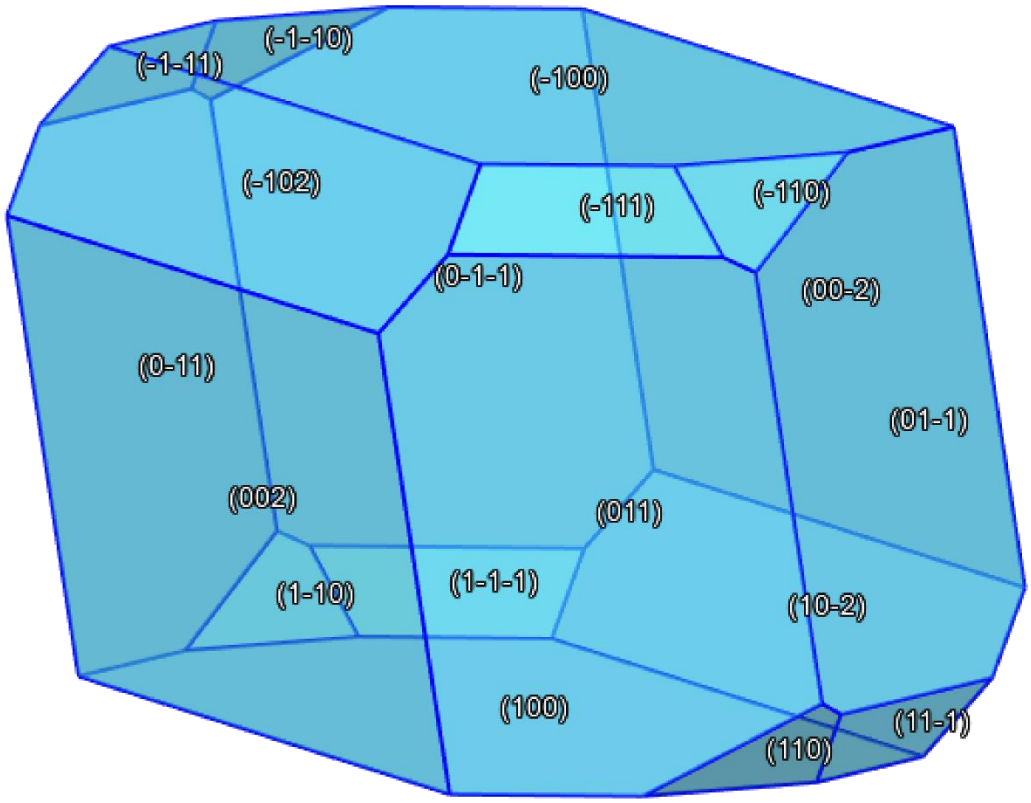

Figure S21. Predicted BFDH morphology for HAN:DAT.

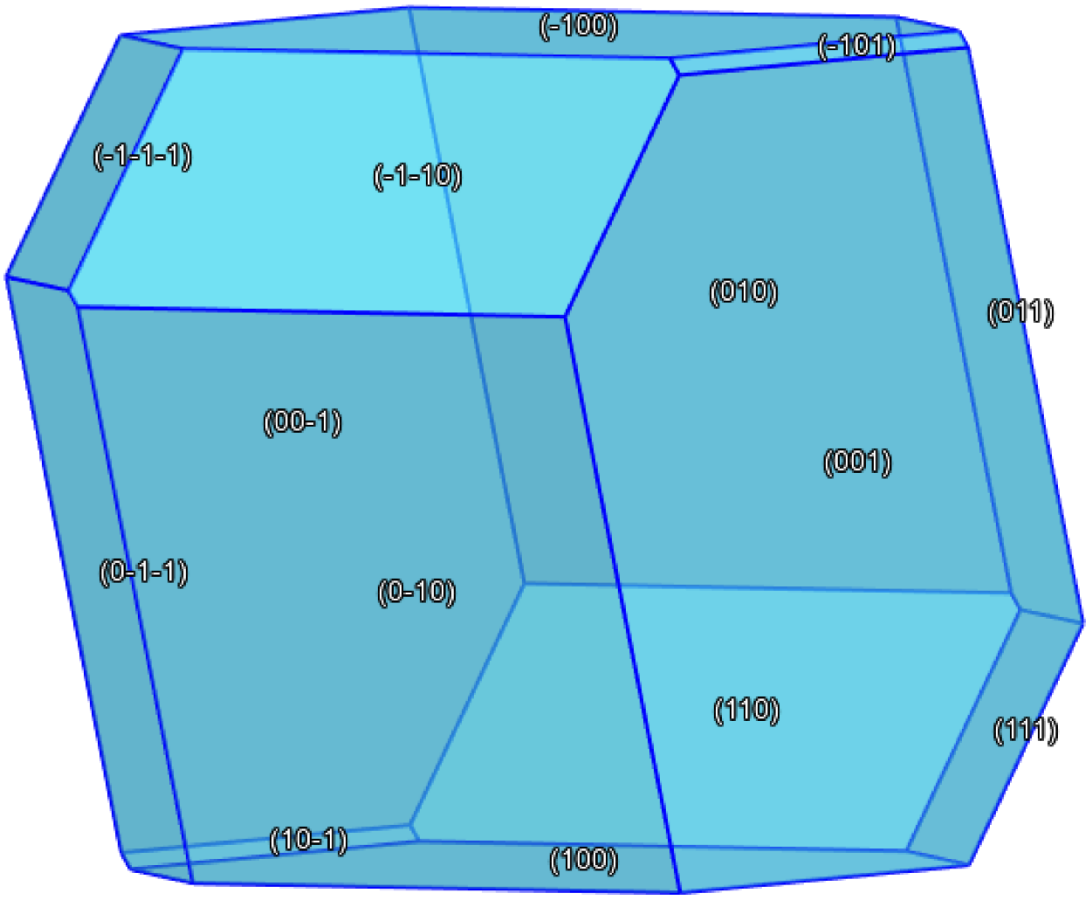

Figure S22. Predicted BFDH morphology for HAN:PA.

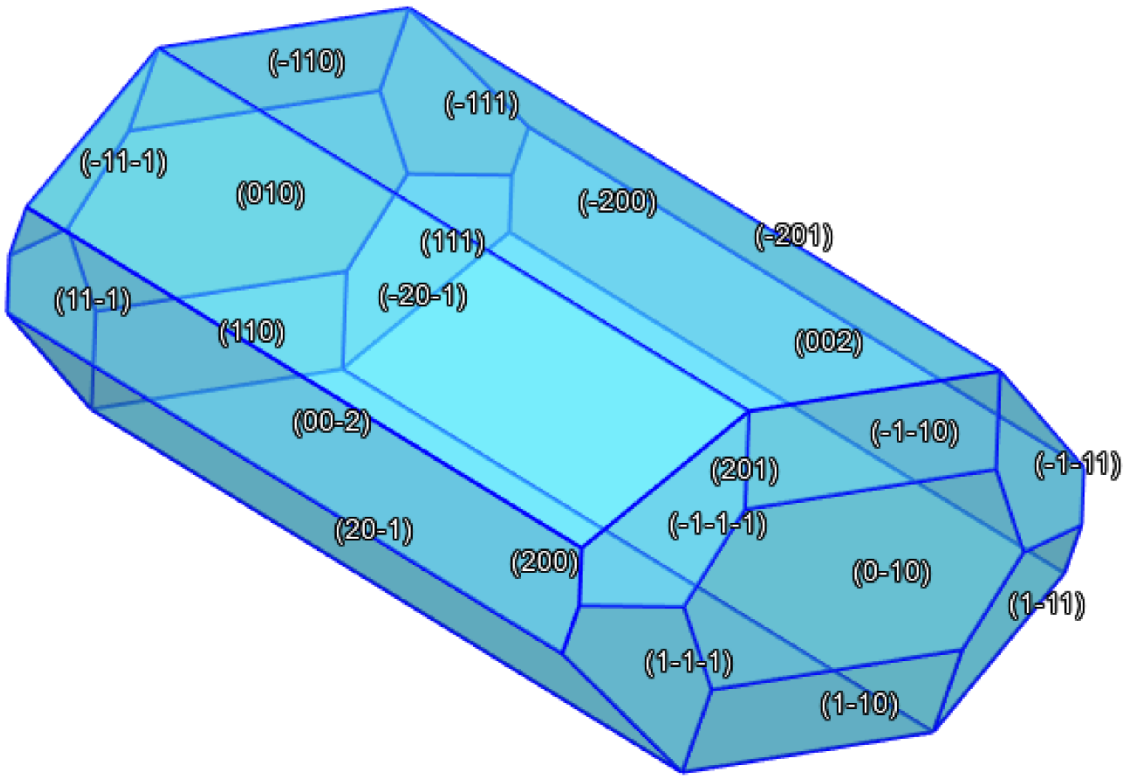

Figure S23. Predicted BFDH morphology for HAN:TO.

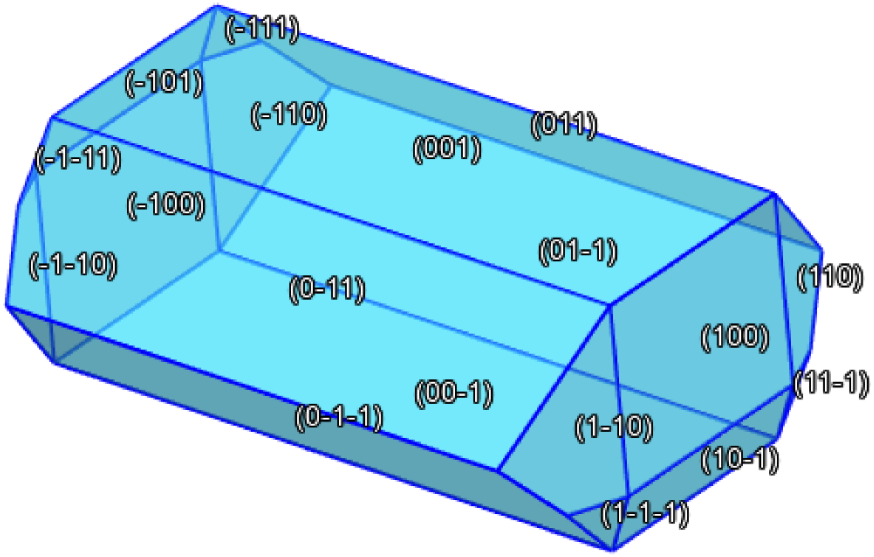

Figure S24. Predicted BFDH morphology for HAN:Urea.

S8. Calculated Formulation Performance

The specific impulse of generic formulations containing HAN energetic cocrystals was calculated and compared to the same formulations containing AP. Calculations were performed using CHEETAH 7.0 at a chamber pressure of 68.046 atm, exhaust pressure of 1 atm, and all compositions at TMD. The heat of formation for the cocrystals was obtained by considering the materials as physical mixtures of the components.

Table S2. Calculated specific impulse for generic propellant formulations containing HAN energetic cocrystals or AP. All formulations are in terms of weight%.

Energetic	**80% Energetic / 20% HTPB**	**70% Energetic / 15 % Al / 15% HTPB**	**70% Energetic / 15 % Al / 15% GAP**
HAN:5-AT	200.0 s	245.4 s	259.1 s
HAN:ANTA	200.1 s	245.3 s	259.5 s
2HAN:PDO	206.1 s	249.7 s	263.3 s
AP	228.6 s	262.0 s	261.4 s

S9. References

1. Scott E. McKay, Joseph A. Sooter, Satish G. Bodige, Silas C. Blackstock. OXIDATION METHODS FOR AROMATIC DIAZINES: SUBSTITUTED PYRAZINE-N-OXIDES, PYRAZINE-N,N'-DIOXIDES, AND 2,2':6',2"-TERPYRIDINE-1,1"-DIOXIDE. Heterocycl Commun. 2001 Aug 1;7(4):307–12.

2. Dolomanov OV, Bourhis LJ, Gildea RJ, Howard J a. K, Puschmann H. OLEX2: a complete structure solution, refinement and analysis program. J Appl Crystallogr. 2009 Apr 1;42(2):339–41.

3. Sheldrick GM. SHELXT – Integrated space-group and crystal-structure determination. Acta Crystallogr Sect Found Adv. 2015 Jan 1;71(1):3–8.

4. Sheldrick GM. Crystal structure refinement with SHELXL. Acta Crystallogr Sect C Struct Chem. 2015 Jan 1;71(1):3–8.